Journal of Zhejiang University-SCIENCE A 2025 26(11):1083-1098
www.jzus.zju.edu.cn; www.springer.com/journal/11582
E-mail: jzus_a@zju.edu.cn

Research Article
https://doi.org/10.1631/jzus.A2400509

Check for updates

Experimental study on vibration source characterization from wheel–rail impacts in urban rapid rail transit turnouts

Zhaoguang ZHENG[1,2], Zihan ZHOU[1,2], Jingmang XU[1,2✉], Zeyu LIU[1,2], Jiayi HU[1,2], Jiayin CHEN[3✉], Ping WANG[1,2]

[1]*MOE Key Laboratory of High-speed Railway Engineering, Southwest Jiaotong University, Chengdu 610031, China*
[2]*School of Civil Engineering, Southwest Jiaotong University, Chengdu 610031, China*
[3]*School of Future Transportation, Guangzhou Maritime University, Guangzhou 510725, China*

Abstract: Many railway turnouts are often installed near metro depots and stations, leading to significant environmental vibrations reaching nearby infrastructure. Vibration in turnout zones can originate from various sources, such as rail joints, wheel-load transitions, uneven stiffnesses, rail corrugation, and small-radius curves. These factors contribute to turnout zones having considerably higher vibration levels than plain track sections. Additionally, in urban rapid transit systems, higher train speeds exacerbate wheel–rail impact excitation, further intensifying such vibrations. Despite turnout zones accounting for a large share of environmental vibrations, there have been few systematic studies on their specific sources and mechanisms in the context of rapid transit systems. This knowledge gap has hindered the development and optimization of vibration mitigation strategies for turnout structures. Therefore, in this study, we investigate five representative sets of turnouts from a rapid transit system in a Chinese city, with train speeds ranging from 80 to 150 km/h. Field tests were conducted on real operating trains, with vibration accelerations measured at turnout rails and tunnel walls. This study systematically examines the effects of turnout structure, train carriage position, speed, and vibration mitigation measures on the vibration source characteristics. Time-frequency methods were employed to analyze the test data. Our findings reveal that when train speeds exceed 100 km/h, leading and trailing carriages passing through turnouts induce low-frequency vibrations below 80 Hz, thus generating vibrations in the human-sensitive frequency range. Moreover, train-induced vibrations in turnout zones are primarily concentrated in three frequency bands: 0–20 Hz (associated with structural and stiffness irregularities in the turnouts), 50–80 Hz (P2 resonance of the wheel–rail system), and 150–200 Hz (natural frequencies of the rails).

Key words: Urban rapid rail transit; Railway turnouts; Vibration source characterization; Vibration mitigation; Time-frequency domain analysis; Wheel–rail impact

1 Introduction

Urban rapid rail transit refers to passenger rail lines that serve metropolitan areas, often linking urban fringes, new suburbs, and airports. As the name suggests, these systems operate at relatively high speeds, typically ranging from 80 to 160 km/h. In contrast, conventional urban rail transit systems operate at lower speeds, generally between 30 and 60 km/h. During operation, the interaction between a train and the track generates significant vibrations. These vibrations can adversely affect the health and quality of life of nearby residents, particularly those living near train stations and depots, as well as compromise the structural integrity of buildings and the functionality of precision instruments (Norgate et al., 2020; Lei et al., 2021; Sadeghi and Vasheghani, 2021). Moreover, environmental vibration pollution tends to be stronger with higher train speeds (Yang et al., 2019; Mathur, 2020; Wang et al., 2020; Gao et al., 2023).

Turnouts are critical components of rail infrastructure, as they enable trains to switch from one track to another. However, they are also one of the weaker points in the rail system (Wen et al., 2014; Xu et al., 2020; Lai et al., 2021; Zheng et al., 2025). Due to

✉ Jingmang XU, mang080887@163.com
Jiayin CHEN, chenjiayin@gzmtu.edu.cn
Zhaoguang ZHENG, https://orcid.org/0000-0002-7309-1009

Received Oct. 29, 2024; Revision accepted Mar. 26, 2025; Crosschecked Sept. 19, 2025

structural irregularities, uneven stiffnesses, rail joints, and potential geometric defects, the impact loads generated as trains pass through turnouts are typically greater than those generated on plain track sections. These loads produce high-frequency impacts, as well as low-frequency environmental vibrations. The aforementioned structural irregularities mainly refer to variations in rail cross-sections and wheel load transitions, which induce impact vibrations in the wheel–rail system. Consequently, environmental vibration issues are often more severe in turnout areas than in plain track areas. In order to reduce environmental vibrations and noise in urban rapid rail transit turnout areas, it is important to investigate the intensity of vibration sources and analyze their mechanisms of action.

Countries with advanced rail transit systems have placed great emphasis on studying the environmental effects of rail-induced vibrations. For example, Japan officially classified vibration as one of the seven major forms of pollution, and has developed methods to predict environmental vibration levels (Takamatsu et al., 1982). Also, the UK has conducted comprehensive research into the relationships between train speed, excitation frequency, track parameters, and resonance phenomena. Like other forms of vibration, rail transit vibrations propagate through shear waves, compressional waves, and surface waves (Sun et al., 2019). The vibration acceleration generated by train operations typically diminishes with increasing distance (Sheng et al., 1999), with the rate of attenuation being strongly influenced by the density and characteristics of surrounding soil layers. Soils with stronger viscoelastic properties tend to exhibit faster vibration decay (Huang et al., 2021), while denser soils can slow the rate of attenuation (Bao et al., 2017). Intuitively, high-frequency vibrations decay more rapidly with distance, whereas low-frequency vibrations persist over longer distances (Chen et al., 2022). In a study on vibration and noise around subway depots, Zou et al. (2015) found that horizontal vibrations near throat areas and curved tracks were significantly stronger than vertical vibrations. However, as the vibrations propagated to surface structures, the vertical components became more pronounced. These results indicate that the vibration source properties, the direction of propagation, the transmission path, and soil conditions all play vital roles in determining vibration attenuation characteristics.

Models for simulating environmental vibrations caused by wheel–rail interactions can be broadly divided into two categories (Bruni et al., 2009). The first category is that of rigid-flexible coupled multibody dynamics models, which consider the flexibility of the rails and structural parts (Qu et al., 2019; Guo et al., 2020). These models are relatively simplified, allowing for faster computation. The second category is finite element model (FEM), in which various track components are discretized for simulation (Connolly et al., 2014; Sun et al., 2018; Sun et al., 2022). While FEM provides higher accuracy, it is computationally intensive, particularly when modelling nonlinear wheel–rail contacts. Due to current computational limitations, multibody dynamics models are more widely used. However, both approaches rely on numerous assumptions, which limit their ability to replicate real-world conditions.

In current urban rail transit environmental vibration assessments, evaluation metrics such as vibration source strength (VSS), vibration dose value (VDV), vibration decibel (VdB), and peak particle velocity (PPV) are commonly used. These metrics primarily characterize the intensity of environmental vibrations by measuring the acceleration or velocity of surrounding structures (Connolly et al., 2016; Auersch et al., 2017; Kouroussis et al., 2019). Most previous studies have focused on the environmental vibration characteristics for plain track sections (Xu et al., 2019; Sheng et al., 2020; Xin et al., 2020), although a few have examined vibration characteristics for turnout areas. Wang et al. (2020) found that the VSS of tunnel walls near the frog area was significantly higher than in the switch area, with lateral vibrations generally exceeding vertical ones. However, their study was limited to train speeds ranging from 30 km/h to 50 km/h. Gao et al. (2023) investigated the transmission of vibrational energy at different cross-sectional locations in subway turnout areas, while Lei et al. (2024) used the continuous wavelet transform to analyze the vibration characteristics during train deceleration through turnouts. Sang et al. (2020) also studied vibration transmission characteristics, analyzing the vibration responses of track slabs and tunnel walls. Additionally, Jiang et al. (2019) compared the vibration characteristics of floating slab tracks and conventional slab tracks in turnout areas.

Vibrations generated by rail transit cause significant environmental noise pollution. The most common approach to mitigating them is active vibration reduction through modification of the track structure. Specific methods include the use of vibration-damping fasteners (Gao et al., 2024), steel-spring floating slab tracks (Zheng et al., 2024), rail vibration dampers (Wang et al., 2022), and trapezoidal sleepers. For turnout areas, additional solutions have been proposed to meet specific vibration reduction needs, such as stiffness homogenization (Wang et al., 2015), and movable-point frogs that eliminate gaps found in fixed frog areas. However, research on specialized vibration reduction techniques in turnout areas remains limited. In common practice, techniques designed for plain track sections are applied in turnout areas, with the use of vibration-damping fasteners and floating slab tracks being most prevalent (Jiang et al., 2019). However, the effectiveness of vibration reduction measures for trains passing through turnouts at various speeds, as well as such methods' adaptability to different turnout structures, remains poorly understood.

Turnouts experience vibrations than plain tracks due to structural irregularities and uneven stiffness, particularly at higher speeds (80–150 km/h), which amplify environmental vibrations. Despite this, the vibration source characteristics in urban rapid rail transit turnout zones have not been systematically studied. Therefore, understanding vibration sources in these areas is essential for informing control strategies for environmental vibrations and noise. In this study, we select five representative turnouts from an urban rapid transit system in a Chinese city, and conduct field tests to investigate the effects of train speed, turnout type, different train carriages, and vibration mitigation measures on environmental VSS. The goal is to better understand methods for reducing vibration and noise in turnout areas, thereby aiding the sustainable development of quieter rail transit systems.

2 Field measurements

2.1 General

This study involved tests on five sets of turnouts in the urban rapid rail transit system of a Chinese city, as shown in Fig. 1 and Table 1. The turnouts include two sets of No. 9 turnouts and three sets of No. 12 turnouts, all of which have similar service durations and exhibit no significant rail corrugation. Among them, three turnouts feature a fixed frog structure, while two have steel spring floating slabs, and one utilizes a Cologne-egg fastener. Trains decelerated while passing through Turnout A, whereas the other turnouts were

Fig. 1 Tested Turnouts A–E

Table 1 Parameters of Turnouts A–E

Turnout	No.	Frog	Vibration mitigation measure	V (km/h)	Train
A	9	Fixed	Ordinary	58–84	8-car Type A
B	9	Fixed	Damping fastener	100	8-car Type A
C	12	Fixed	Floating slab	100	8-car Type A
D	12	Movable-point	Ordinary	150	4-car Type A
E	12	Movable-point	Floating slab	150	4-car Type A

V represents the speed of the train passing through the turnout traversed at a constant speed. The ordinary turnouts employed Type II fasteners and a monolithic track bed structure, with no vibration mitigation measures implemented. The trains in the tests consisted of either eight- or four-car Type A trains, which passed through the turnouts in reverse directions.

2.2 Measurement methodology

Testing cross-sections were established at different locations within the turnout area, as shown in Fig. 2. This is because the structural characteristics of the turnout area change along the line, for instance, with multiple rails sharing a single baseplate, and different joints and gaps present. Each turnout was tested at three cross-section locations: (I) the joint before the switch, (II) the switch area, and (III) the frog area. For example, the first measurement point in section I of turnout set A was labelled AI-1, with other points following a similar naming convention. Vertical acceleration measurements were made on both the rail and tunnel wall at all three cross-section locations. Given that wheel load transitions in the switch and frog areas tend to increase lateral vibrations, lateral acceleration was also measured in these areas. In the switch area, vertical acceleration was recorded at the curved stock rail before, during, and after the wheel load transition. In the frog area, vertical acceleration was measured on the wing rail before and during the wheel load transition. Following conventions for VSS testing of plain track sections, vibration sensors on the tunnel wall were placed 1.25 m above the rail surface. Each set of turnouts was tested for one full day.

The employed data acquisition device was the INV3060S (China Orient Institute of Noise & Vibration). Accelerometers with a range of 1000*g* were mounted on the rail, while 1*g* accelerometers were installed on the tunnel wall. Data were sampled at a frequency of 12.8 kHz, with each sampling trigger lasting 20 s. Since the tested turnouts are located near platforms, the experimental tunnel has a rectangular cross-section. The test plan was developed in accordance with the ISO 10815-2016 standard (ISO, 2016).

2.3 Measurement indices

The method for calculating the vibration level is described in Section S1 of the electronic supplementary materials (ESM).

According to the CJJ/T 191-2012 standard (Xin et al., 2020), evaluations of tunnel wall vibrations are based on the weighted vibration level in the frequency range of 1 Hz to 200 Hz. It is important to note that for low-frequency environmental vibrations, the characteristic wavelength is typically over 1 m.

2.4 Typical time-domain data

Using the recorded time-domain data from Turnout A as an example, Fig. 3 illustrates typical time-domain vibration data for the rail and tunnel wall in rapid urban rail transit. The subplots represent the vibration acceleration in the following areas from top to bottom:

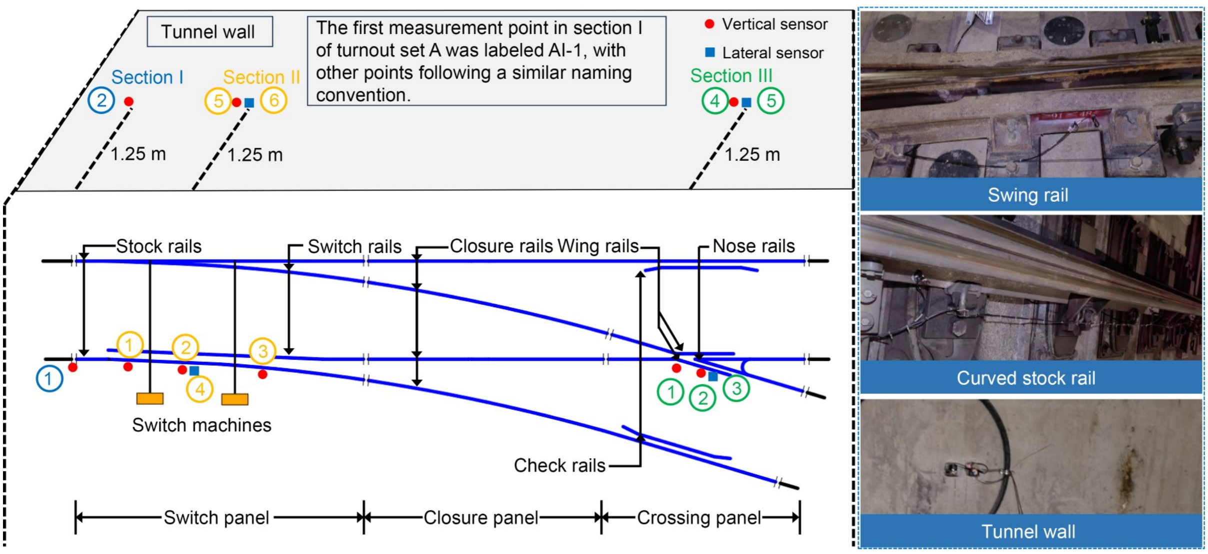

Fig. 2 Acceleration measurement points (1–6) in the turnout area. References to color refer to the online version of this figure

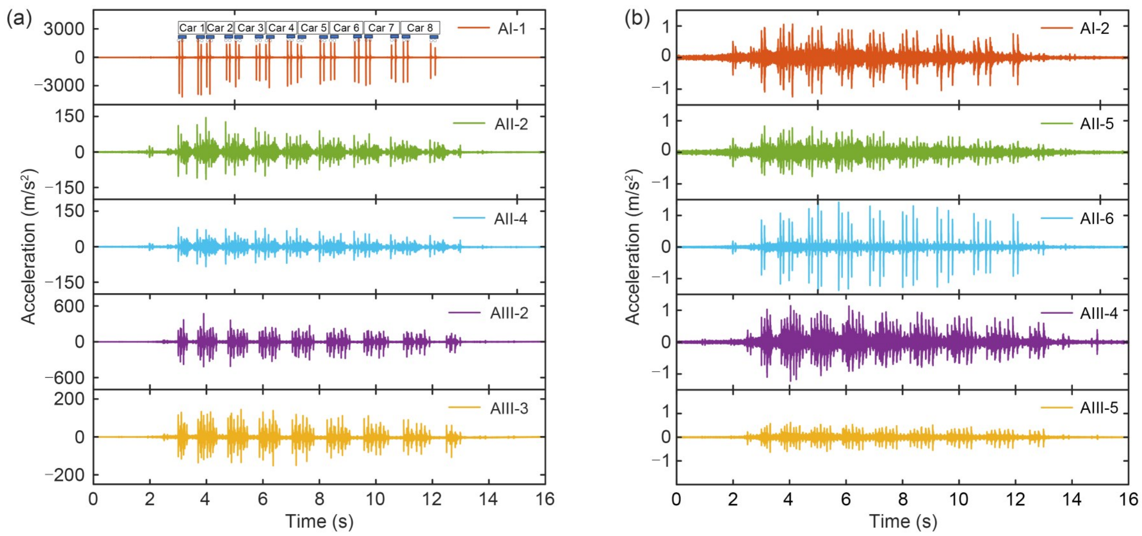

Fig. 3 Time-domain signals of vibration acceleration in Turnout A: (a) rail; (b) tunnel wall

(I) rail joint, (II) switch area-vertical or switch area-lateral, and (III) crossing area-vertical or crossing area-lateral. Significant differences in vibration data are observed at the three measurement cross-sections. In Fig. 3a, the peak acceleration values at the five measurement points on the rail are 4162 m/s^2, 145 m/s^2, 84 m/s^2, 470 m/s^2, and 152 m/s^2, with corresponding root mean square (RMS) values of 57.5 m/s^2, 6.6 m/s^2, 4.9 m/s^2, 20.0 m/s^2, and 8.7 m/s^2. In Fig. 3b, the peak acceleration values at the five measurement points on the tunnel wall are 1.24 m/s^2, 0.83 m/s^2, 1.43 m/s^2, 1.22 m/s^2, and 0.63 m/s^2, with effective values of 0.096 m/s^2, 0.072 m/s^2, 0.064 m/s^2, 0.122 m/s^2, and 0.052 m/s^2, respectively.

Turnout A features a frozen joint design, but still has rail gaps of less than 3 mm. As a result, the peak vibration acceleration at the joint is significantly higher before the turnout than in other areas. When a train passes through at a speed of 80 km/h, the peak acceleration of the rail can reach 416*g*. The next highest values are recorded in the wing rail and curved stock rail. In both the frog and switch areas, the peak vertical accelerations of the curved stock rail and wing rail are greater than the peak lateral accelerations. This indicates that vertical vibrations dominate over lateral vibrations when the train passes straight through the turnout.

In terms of RMS acceleration, the vertical acceleration of the rail at the joint and the wing rail in the frog area is significantly greater than at other measurement points. However, after the vibrations are transmitted to the tunnel wall, the differences in effective acceleration values across measurement points diminish. This is because the impacts primarily generate high-frequency energy, which attenuates significantly as it is transmitted to the tunnel wall. Despite this, the vertical acceleration on the tunnel wall remains the highest in the frog area, which is attributed to the presence of multiple joints and gaps in this cross-section.

In Fig. 3b, the acceleration signals of both the rail and the tunnel wall in the switch area showcase periodicity. This periodicity is caused by the impacts that are generated at the joint and transmitted to the switch area. Moreover, this phenomenon indicates that multiple excitation sources within the switch area interact, resulting in vibrations on the tunnel wall that stem from the superposition of various sources. Additionally, in the frog area, the presence of two joints and a gap generates multiple impact signals in the rails as the wheels pass through.

3 Results and analysis

3.1 Vibration level analysis

3.1.1 Vibration levels at different frequencies

In this section, we analyze the acceleration levels on the tunnel wall within the frequency range of 1 Hz to 200 Hz. Specifically, Turnout A has 27 datasets, Turnout B has 20, Turnout C has 10, Turnout D has 7, and Turnout E has 8. The difference in test data quantity among turnouts is attributed to varying traffic densities associated with each train type. Each dataset represents 20 s of measurement as a single train passes through the given turnout. Fig. 4 presents the frequency-weighted acceleration levels on the tunnel walls for the five different turnouts. The frequency-weighted calculation is based on the acceleration spectrum, with the center frequencies of 1/3-octave bands plotted as the horizontal axis. The shaded areas represent the standard deviation, while the lines indicate average values.

As illustrated in Fig. 4, the standard deviations of vibration levels across the five turnouts are relatively low. While some errors exist in the calculations for frequencies below 20 Hz, the errors for vibration levels above 20 Hz are minimal. This consistency can be attributed to the favorable service conditions of the tested turnouts, which show no significant rail corrugation.

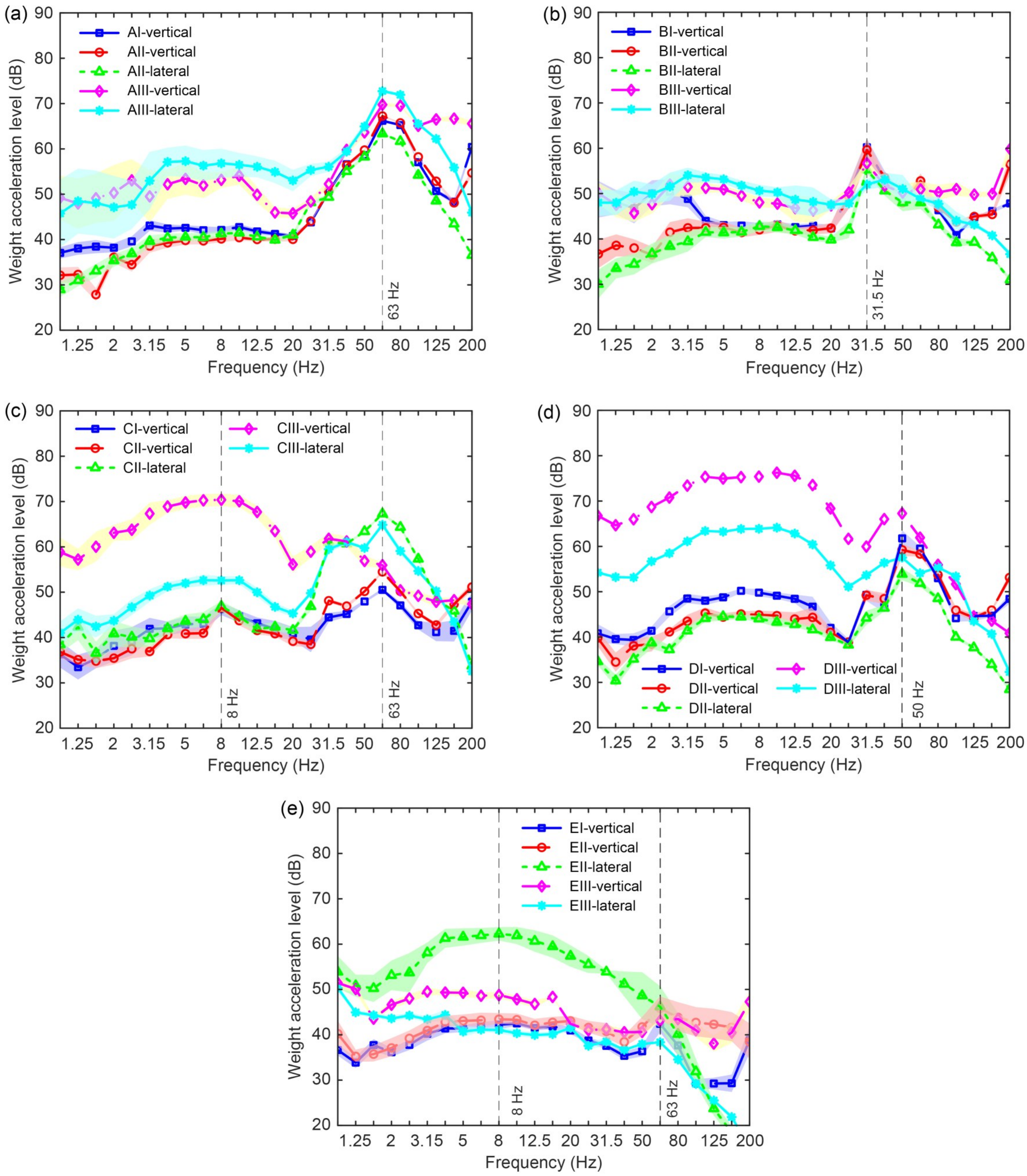

Fig. 4 Acceleration levels of turnouts at different frequencies on tunnel walls. (a)–(e) correspond to Turnouts A–E, respectively

Furthermore, the trains are equipped with an automatic driving system that maintains consistent speed when traversing the turnouts, thereby reducing the variability of the vibrations.

As shown in Fig. 4, by comparing the vibration levels on the tunnel wall at the three cross-section locations—joints, switch area, and frog area—it is evident that the vibration levels in the frog area are generally the highest. Furthermore, the vibration levels at the joint and switch area are quite similar. This can be attributed to the pronounced structural irregularities in the crossing panel, and to the fact that the stiffness is 1.5–3 times greater than that of the closure panel. While the joint area has higher peak vibration acceleration, it primarily generates high-frequency vibrations, which attenuate quickly and have a relatively minor impact on the tunnel wall.

When the train passes through the No. 9 fixed-frog Turnout A, the peak vibration on the tunnel wall occurs at 63 Hz. The value of this peak is attributed to the P2 resonance of the wheel–rail system. Turnout B utilizes Cologne-egg fasteners, resulting in a peak vibration on the tunnel wall at 31.5 Hz. Compared to Turnout A, Turnout B exhibits a lower natural vibration frequency. This is due to the reduced vertical stiffness of the fasteners, which causes a lower frequency for the wheel–rail system's P2 resonance.

When a floating slab is utilized beneath the turnout, the tunnel wall vibration exhibits two distinct peaks at 8 Hz and 63 Hz. The peak at 8 Hz is due to the resonance of the floating slab. A comparison between Turnout A and Turnout D (No. 9 and No. 12) reveals that Turnout D has significantly lower vibrational energy above 31.5 Hz, and higher environmental vibrational energy below 20 Hz. Notably, the peak tunnel wall vibration for Turnout D occurs at 50 Hz. This peak is likely due to the use of vulcanized pads, which have lower stiffness than conventional under-plate pads. Additionally, trains traversing Turnout D operate at significantly higher speeds than those passing through Turnout A. Thus, with the use of movable-point frogs, turnout No. 12 effectively reduces high-frequency vibrational energy above 31.5 Hz, but is less effective in mitigating low-frequency vibrations below 20 Hz.

Comparing Turnout C (fixed frog No. 12 turnout) and Turnout E (movable-point No. 12 turnout), it is clear that the tunnel wall vibration levels at Turnout E are significantly lower than those at Turnout C, particularly in the frog area. This reduction is primarily due to the movable-point design of Turnout E, which stands in contrast to the fixed-frog configuration in Turnout C.

As shown in Fig. 4, with greater train speed, the proportion of low-frequency environmental vibrations (below 20 Hz) in the overall vibrational energy increases significantly. Similarly, Auersch et al. (2017) studied railway-induced vibrations on surface lines in Sweden, and found that as train speed increased, the amplitude of the axle-box acceleration grew more significantly in the low-frequency range. The primary reason for this phenomenon is that at low speeds, the vibration frequency induced by quasi-static track deflection is extremely low, and the coupled vibration of the wheel–rail system dominates. However, when the train speed exceeds 100 km/h, quasi-static rail deflection becomes the dominant factor influencing wheel–rail vibrations under 25 Hz (Thompson, 2010).

From Fig. 4, it is evident that the low-frequency vibration levels of Turnouts C and D are significantly higher in the frog area compared to other regions; the vibrations below 20 Hz appear to dominate. This is likely because the structural irregularities and abrupt stiffness variations in the frog area cause more intense wheel–rail impacts compared to other areas. Furthermore, these excitation mechanisms are intimately related to train speed. It is important to note that Figs. 4c–4e correspond to the No. 12 turnout, while Figs. 4a and 4b correspond to the No. 9 turnout. The No. 12 turnout, which has a longer wheel load transition range, may generate stronger low-frequency disturbances than the No. 9 turnout, especially at higher speeds. In Turnout E, the lateral vibration levels below 20 Hz within the switch area are greater than the vertical levels in the frog area. This phenomenon can be attributed to three main factors. Firstly, the train speed is relatively high. Secondly, a floating slab track system was used. Finally, the tunnel wall dimensions in Turnout E are quite different from those at other measurement points, showcasing large open-cut voids (Fig. 1).

3.1.2 Frequency-weighted vibration levels

The vibration levels at various cross-section locations for the five turnout sets are presented in Fig. 5, with the standard deviation of the data indicated by error bars. The acceleration levels on the tunnel wall in the switching area of Turnout A show that the standard deviation of the vertical vibration level is only

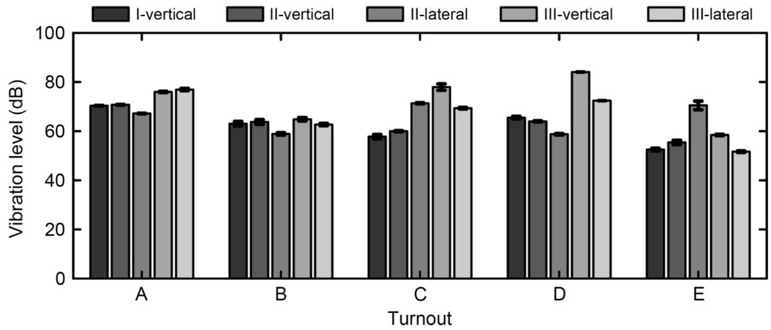

Fig. 5 Vibration levels on the tunnel wall for the different turnouts

0.11 dB, while the standard deviation of the lateral vibration level is 0.14 dB. These low standard deviations indicate minimal differences between the test datasets, signifying good measurement accuracy.

From Fig. 5, it is evident that environmental vibrations vary due to differing turnout types, mitigation measures, and cross-section locations. At the three cross-sectional positions from Turnouts A to D, the vibration level in the frog area is consistently the highest. Moreover, the vertical vibration levels at the switch and joint areas are quite similar. In contrast, Turnout E exhibits the greatest lateral vibration levels on the tunnel wall in the switch area. When comparing Turnout A and Turnout B, there are reductions in vibration levels ranging from 7 dB to 14 dB, with the most significant damping effect observed in the frog area. This highlights the superior damping performance of the Cologne-egg fasteners. Additionally, the larger cross-sectional dimensions of the tunnel at Turnout B significantly contribute to the lower vibration levels.

Compared to Turnout A, Turnout C exhibits better vibration reduction at the joint and switch cross-sectional positions, with reductions ranging from 10.7 dB to 12.6 dB. However, its damping performance is poorer for lateral vibrations on the tunnel wall in the switch area, and vertical vibrations in the frog area. Experimental data from Turnouts D and E reveal that even with only the movable-point rail in the frog area, significant environmental vibrations are generated when trains traverse the turnouts at high speeds. Notably, the vertical vibration level in the frog area of Turnout D reaches 84.1 dB, making it the highest among the five turnouts. Turnout E incorporates a movable-point frog along with a floating slab track, leading to effective vibration reduction in the frog area.

The vertical vibration levels in the switch and frog areas are often higher than the lateral vibration levels, which may be due to the stronger vertical wheel–rail impacts that occur when traversing the turnout on the through route compared to the diverging route. However, data from Turnouts C and E indicate that lateral vibrations in the switch area are considerable. This phenomenon can be attributed to the design of floating slabs, which primarily mitigate vertical vibrations. Consequently, the lateral vibrations in the switch area of the tunnel wall surpass the vertical vibrations. Specifically, Turnout C exhibits 11.4 dB higher lateral vibration levels, while Turnout E's levels are 15.1 dB higher.

Turnouts A to C utilize frozen joints, whereas Turnouts D and E employ welded joints. As discussed in Section 2.4, the rapid passage of trains over frozen joints induces strong rail vibrations that propagate into the environment. Observing the results in Fig. 5, the tunnel wall vibration level at the joint location for Turnout D is 4.8 dB lower than that of Turnout A. Additionally, the vibration level in Turnout E is 5.3 dB lower than in Turnout D. This demonstrates that using welded joints effectively reduces environmental vibrations during rapid train passage.

The peak factors of the rail acceleration signals measured at the joints for Turnouts A, C, and D are presented in Fig. S1 in the ESM. A total of 10 datasets were calculated for Turnouts A and C, while seven datasets were calculated for Turnout D. The peak factor is determined by dividing the peak acceleration by the RMS value over the test duration. For Turnouts A and C, the trains consisted of eight carriages, and 20 s of data was used. In contrast, the train passing through Turnout D had only four carriages, resulting in 10 s of data being used. The results indicate that the peak factors for welded joints are significantly lower than those for frozen joints. This finding suggests that welded joints perform better in reducing impact vibrations.

3.2 Time-frequency analysis

Details on the calculation of the continuous wavelet transform (CWT) can be found in Section S2.2 of the ESM.

By applying the CWT, the acceleration signals on the tunnel walls at the various turnouts are converted into the time-frequency domain. Each set of turnouts is displayed in five subplots, as presented in Fig. 6. The horizontal axis represents time, the vertical axis represents frequency, and the color scale indicates the magnitude of the acceleration following wavelet decomposition. In Fig. 6, bright spots or lines highlight peak vibrations within specific time and frequency ranges.

Overall, the vibrational energy in the frog area exhibits a wider frequency bandwidth, with the maximum vibration response occurring in this area. In Turnout A, as the train speed decreases from 84 km/h to 58 km/h while traversing the turnout, the frequency bandwidth of the induced vibrations on the tunnel wall noticeably narrows from 40–120 Hz to 50–80 Hz, with the center frequency shifting lower. This bandwidth is primarily associated with the P2 resonance of the wheel–rail system. Above 150 Hz, significant energy is concentrated on the tunnel wall. This is attributed to structural irregularities in the turnout, which generate relatively high-frequency impacts as the train passes by.

In Turnout B, the use of Cologne-egg fasteners results in a notable frequency band around 30 Hz in the time-frequency results of the vibration acceleration on the tunnel wall, as depicted in Fig. 6b. This phenomenon is attributed to the low stiffness of the damping fasteners, which induces resonance in the wheel–rail system at lower frequencies.

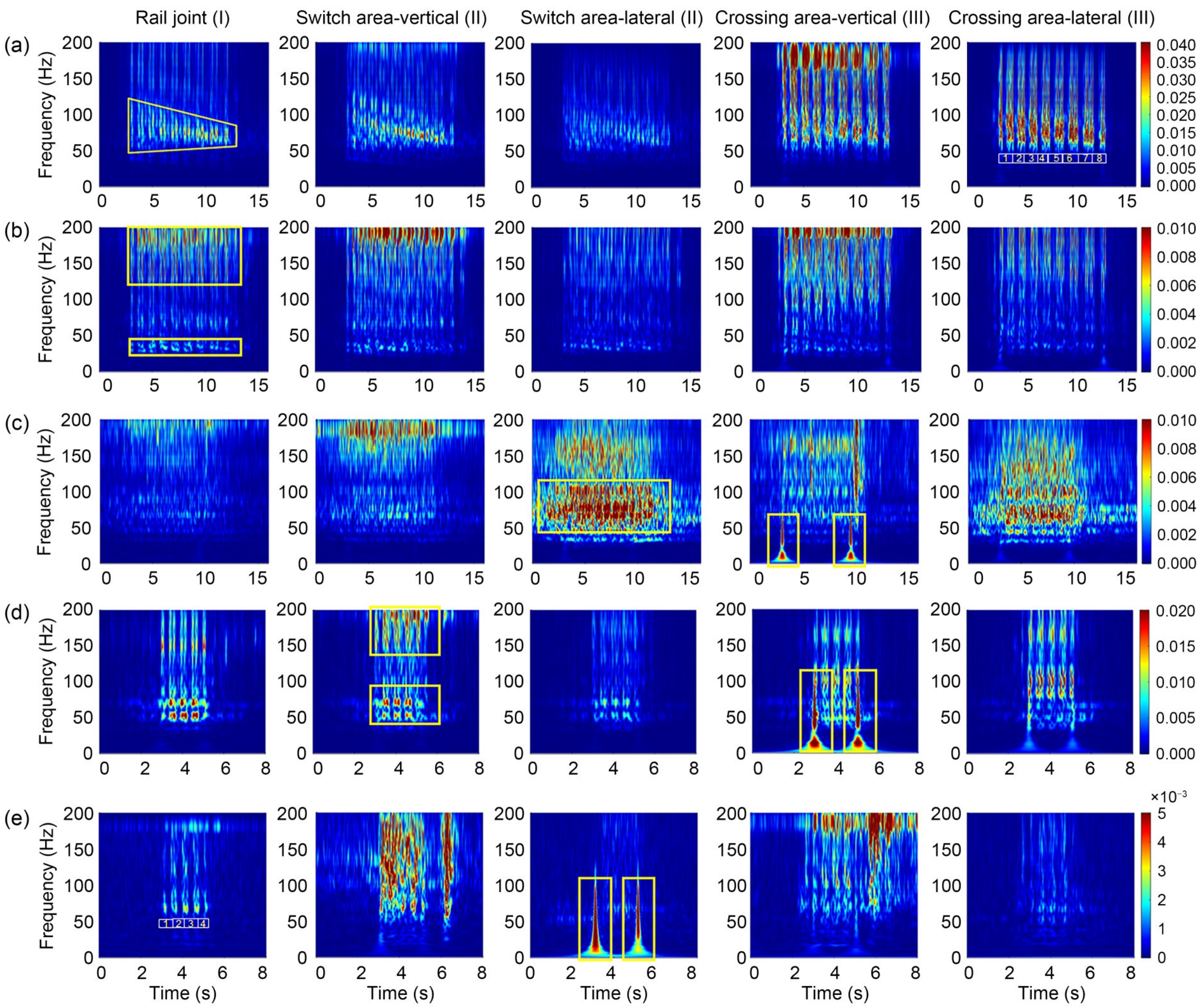

Fig. 6 Time-frequency representation of acceleration signals on the tunnel wall, with (a)–(e) representing Turnouts A–E. The legend is the wavelet coefficient (m/s²). References to color refer to the online version of this figure

Turnout C utilized steel spring floating slabs for vibration damping. In contrast to Turnout A, vertical vibrations on the tunnel wall were effectively suppressed. However, the amplitude of the lateral vibrations significantly exceeded that of the vertical vibrations. Notably, during the passage of the leading and trailing trains, bright spots appeared in the vertical vibrations below 20 Hz on the tunnel wall in the frog area. Similar phenomena were observed in the vertical and lateral accelerations in the frog area of Turnout D, as well as in the lateral accelerations in the switch area of Turnout E. Since this phenomenon did not occur at the joints, it may be related to inherent structural and stiffness irregularities in the switch and frog areas of the turnouts. Furthermore, leading and trailing carriages tend to sway more than middle carriages (Zhou et al., 2017), which may excite stronger low-frequency signals.

3.3 Vibration sources induced by passage of different carriages through the turnouts

From the time-frequency analysis results in Section 3.2, we know that when the train speed exceeds 100 km/h, environmental vibrations induced by the leading and trailing carriages differ significantly from those caused by the middle carriages. To further investigate these differences, we calculated the vibration levels for five sets of turnouts as various carriages passed, as shown in Fig. S2 of the ESM. The previous time-domain data analysis indicated that the train generates substantial periodic impact signals while traversing the turnout. This characteristic can be used to differentiate data from different carriages. In cases where the time-domain data are difficult to distinguish, the wavelet coefficient decomposition method (Gao et al., 2023) can be employed to extract high-frequency signals. This approach allows for better identification of the times when different carriages pass.

As depicted in Fig. S2a of the ESM, the vibration levels at the five measurement points on Turnout A exhibit an increasing trend for the first three carriages. Combined with the previous wavelet transform analysis, it is evident that at relatively high speeds, the acceleration signals transmitted to the tunnel wall do not immediately dissipate. Consequently, after attenuation, the vibration signals generated by the first carriage overlap with the environmental vibrations caused by the second carriage. This results in a gradual increase in vibration levels from the first to the third carriage. As the remaining carriages pass, the train’s speed decreases, leading to reduced vibration levels on the tunnel wall near the turnout. This decrease is particularly pronounced in the vertical vibrations at the frog area and joint. Conversely, the reduction is less significant at the other three measurement points. This observation suggests that the environmental vibrations induced at the frog and joint areas are more sensitive to changes in train speed.

In Turnouts B to E, distinct characteristics of the environmental vibration sources emerge as train speeds exceed 100 km/h. In the frog and switch areas of the tunnel walls, the vibrations induced by the leading and trailing carriages are substantially higher than those caused by the middle carriages. For instance, on the tunnel wall in the frog area of Turnout B, the lateral vibration level generated by the leading and trailing carriages is approximately 10 dB higher than that of the middle carriages. In Turnout C, the vertical vibration at the frog area shows a difference of 33 dB when comparing the leading and trailing carriages with the middle carriages. In Turnout D, the vertical vibration level on the tunnel wall is about 34 dB higher for the leading and trailing carriages, while the lateral vibration difference is approximately 12 dB. In the switch area of Turnout E, the difference in lateral vibration level can reach up to 50 dB. It is important to note that these substantial vibration level differences between carriages were not observed at the joints. Accordingly, this phenomenon is not attributed to the impact between the wheels and rails resulting from increased speed.

Taking the vertical vibrations of the wing rail and tunnel wall in Turnout D as an example, we analyzed the frequency distribution of vibration energy for different bogies (rotating chassis under rail vehicles) as they passed through the turnout; the results are illustrated in Fig. 7. It is clear that the acceleration vibrations induced in the wing rail at the frog area are primarily concentrated in three frequency bands: below 20 Hz, around 50 Hz, and above 120 Hz. In the first and second frequency bands, significant differences in vibration levels are observed between the leading and trailing bogies compared to the middle bogies, while the differences in the third band are relatively small. This indicates that the higher vibration levels of the leading and trailing bogies are mainly attributed to strong low-frequency vibrations, especially those below 80 Hz.

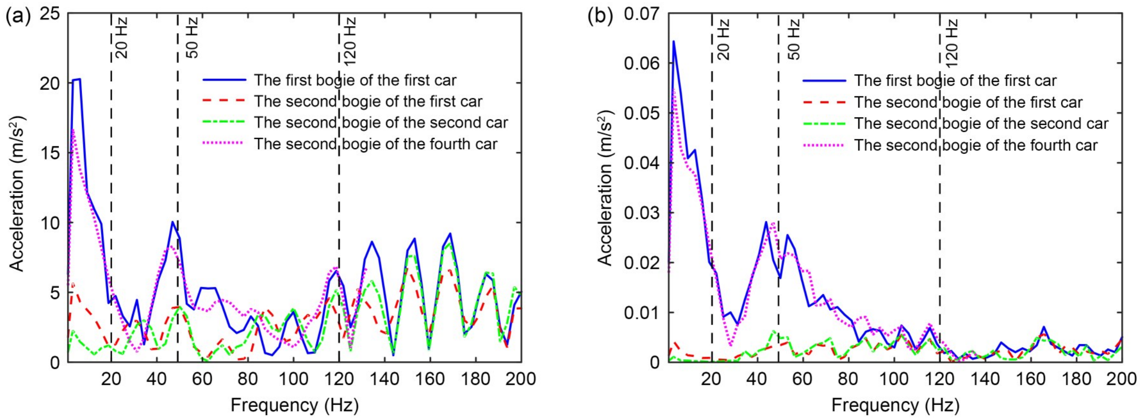

Fig. 7 Acceleration spectra generated by different bogies passing through the turnout: (a) wing rail (DIII-2); (b) tunnel wall (DIII-4)

As the vibrational energy is transmitted to the tunnel wall, the energy above 120 Hz decays significantly, whereas the energy in the first and second bands decays more slowly. Thus, targeting these two bands in environmental vibration assessments and mitigation efforts may be useful. Notably, the first-order vertical bending modal frequency of the turnout rail is primarily concentrated between 100 Hz and 200 Hz. This implies that the vibrational energy in the range of 120 Hz to 200 Hz may be closely related to the resonance of the turnout rails. Furthermore, the second band (near 50 Hz) is close to the P2 resonance frequency of the wheel–rail system.

To further investigate the source of low-frequency vibrational energy generated by the leading and trailing carriages (below 80 Hz), we plotted the time-domain acceleration signals for the wing rail and tunnel wall of Turnout D, as shown in Fig. S3 of the ESM. One can observe significantly low-frequency signals occurring at 3 s and 5.09 s, which correspond to the passage of the first and last wheelsets, respectively. Notably, these signals do not appear at the precise moment of load transfer; instead, they emerge slightly before it. Therefore, we hypothesize that the generation of these low-frequency signals may be related to structural irregularities at points in the turnout where the wheel load transition begins.

Using the synchronous wavelet transform, which provides higher time-frequency resolution (Daubechies et al., 2011), we analyzed the acceleration signals on the wing rail and tunnel wall for the first bogie passing through the frog area of Turnout D. The results are presented in Fig. S4 of the ESM. From Fig. S4a, it is evident that during the wheel load transfer, the induced impacts are primarily concentrated above 120 Hz, with the P2 resonance frequency being observed around 50 Hz. Prior to the wheel load transfer, the excitation of signals mainly occurs in the low-frequency range, below 80 Hz. When these vibrations are transmitted to the tunnel wall, high-frequency signals above 120 Hz experience significant attenuation, while low-frequency signals below 80 Hz experience relatively little decay. Moreover, our analysis indicates that the central frequency of the low-frequency vibrations below 20 Hz occurs at 3 s, while the first wheelset passes the measurement point at 3.05 s. Using a train speed of 150 km/h, the location of the low-frequency disturbance is approximately 2 m before the wheel load transfer position. This location corresponds to the point where the stock rail transitions to the wing rail, resulting in low-frequency disturbances from interactions between the wheel and the wing rail.

To evaluate the vibrational energy present in different frequency bands, the following energy evaluation indicator is proposed:

$$E(t)=\sum_{f=f_1}^{f_2} C(f,t), \tag{1}$$

where t is the time, f_1 and f_2 are the lower and upper limits of the frequency band, respectively, and $C(f, t)$ represents the wavelet coefficients obtained after performing the synchronous wavelet transform.

Calculated values of the energy evaluation indicator at various times are shown in Fig. 8. At frequencies below 50 Hz, the vibrational energy of the first

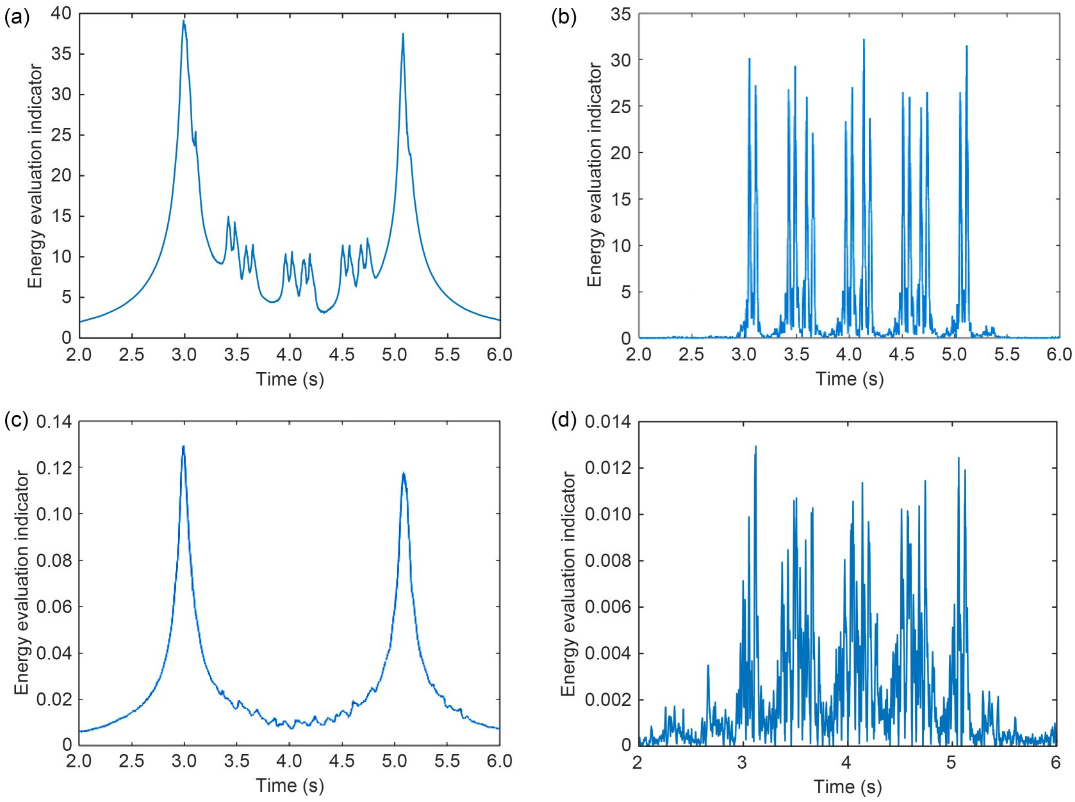

Fig. 8 Vibrational energy distribution caused by the passage of different carriages: (a) rail 0–50 Hz, DIII-2; (b) rail 120–200 Hz, DIII-2; (c) tunnel wall 0–50 Hz, DIII-4; (d) tunnel wall 120–200 Hz, DIII-4

and last carriages is significantly greater than that of the middle carriages. Additionally, there is a marked difference in energy distribution when comparing the first and last carriages with the middle ones. As vibrations transmit from the rails to the tunnel wall, this disparity becomes even more pronounced. In contrast, the differences in vibrational energy between carriages are minimal within the range of 120 Hz to 200 Hz. Consequently, the environmental vibrations transmitted to the tunnel wall do not differ significantly.

3.4 Discussion

In urban rapid rail transit, using frozen joints in turnouts can generate substantial impacts with maximum acceleration peaks exceeding 400*g*. This is significantly higher than test results observed on conventional tracks (Gao et al., 2023). In contrast, utilizing welded joints effectively reduces such impacts, leading to decreased source strength of the environmental vibrations; this approach achieves a damping effect of approximately 5 dB.

To analyze the impact of wheel load transition on environmental vibrations, we examine the energy distribution of the rail in the switch area across the 0–80 Hz frequency range, as shown in Fig. 9. Fig. 9a illustrates the trace of the wheel–rail contact points in the turnout structure, so as to clarify the changes in the wheel–rail contact point caused by inherent structural irregularities in the turnout. The horizontal axis represents mileage (longitudinal coordinate), while the vertical axis shows the vertical coordinate of the wheel–rail contact point. The inherent structural irregularities in the turnout primarily result from factors such as asymmetric rails with variable cross-sections, multiple rails sharing a single tie plate, variations in the size of the tie plate along the track, complex boundary conditions, and auxiliary components like fillers and iron blocks. Figs. 9b–9d reveal that at rail head widths of 18 mm and 55 mm (which correspond to the start and end positions of the wheel load transition from the switch rail to the stock rail, respectively), the vibrational energy of the rail significantly increases at frequencies below 80 Hz. The locations of the wheel load transitions were determined based on observed conditions of the bright bands at the field site. At a rail head width of 40 mm, the vibrational energy is markedly reduced,

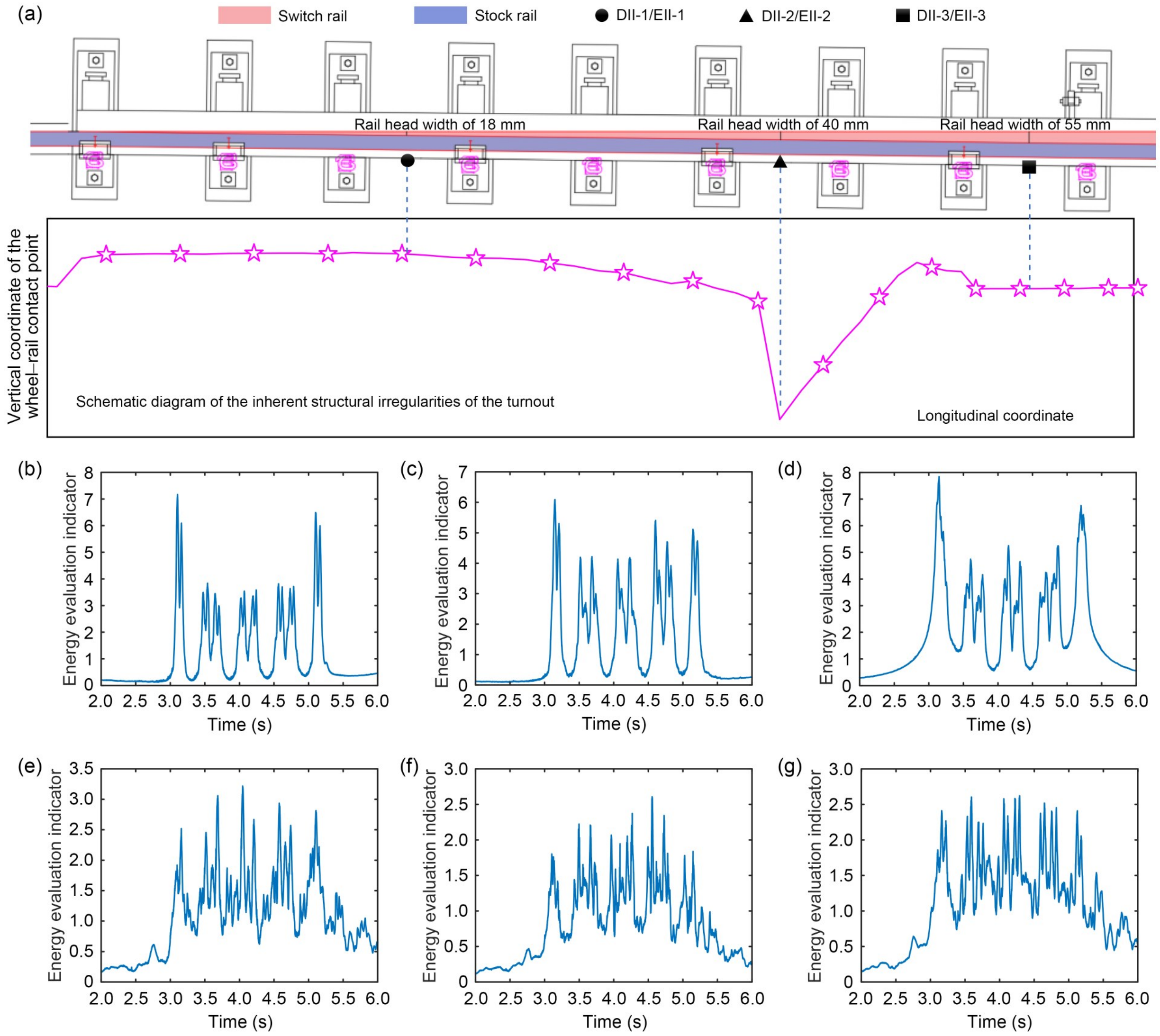

Fig. 9 Vibrational energy of the rail under wheel load transition in the switch area at frequencies below 80 Hz: (a) the distribution of measurement points on the curved stock rail and a schematic of the structural irregularities in the turnout; (b)–(d) turnout D, DII-1 to DII-3; (e)–(g) turnout E, EII-1 to EII-3

especially during the passage of the first and last carriages. Therefore, when attempting to manage the vibrational energy generated in the switch area, it is essential to consider the vibration characteristics throughout the entire wheel load transition. A comparison of the test data from Turnouts D and E indicates that employing a floating plate structure effectively reduces the vibrational energy in the rail during wheel load transitions at frequencies under 80 Hz. This approach is particularly effective in suppressing the vertical low-frequency excitations induced by the first and last carriages.

Comparing these findings with previous studies (Wang et al., 2020; Gao et al., 2023), it is evident that the frequency distributions of environmental vibrations in rapid rail transit turnout areas differ significantly from those in low-speed turnouts. When trains cross turnouts at speeds exceeding 100 km/h, the first and last carriages tend to induce strong environmental vibrations below 80 Hz, particularly within the 20 Hz range. This phenomenon primarily stems from the displacement of the wheel–rail contact points, caused by changes in the spatial positioning and cross sections of the rails in the switch and frog areas. Such changes contribute to structural irregularities in the turnout region. Furthermore, the maximum vibration level on the walls of the turnout tunnel is likely associated with low-frequency energy below 20 Hz, originating from the frog or switch area.

Based on the experimental results, we suggest adopting welded joints and movable-point frogs in urban rapid rail transit systems to mitigate vibration in turnouts. Furthermore, vibration control measures should prioritize reducing the low-frequency vibrations under 20 Hz, especially when train speeds exceed 100 km/h.

4 Conclusions

This study investigated the VSS characteristics of turnouts in urban rapid transit systems, specifically for train speeds ranging from 80 to 150 km/h. Vibration acceleration measurements were made on rails and tunnel walls for five different sets of turnouts.

The VSS measured during turnout traversal could be divided into three frequency bands within 200 Hz: 0–20 Hz, 50–80 Hz, and 150–200 Hz. These bands represent three different vibrational sources, namely turnout structural and stiffness irregularities (0–20 Hz), the P2 resonance of the wheel–rail system (50–80 Hz), and the turnout rail resonance (150–200 Hz). When the train speed exceeds 100 km/h, the peak energy of environmental vibrations in the frog and switch areas may shift from the second to the first frequency band. Moreover, when train speeds exceed 100 km/h, the leading and trailing carriages can induce substantial low-frequency vibrations (below 80 Hz) in the turnout's switch and frog area. Additionally, the difference in vibration levels between different carriages can reach up to 50 dB. This phenomenon is closely related to the wheel–rail impacts that occur during the wheel load transition.

With the application of Cologne-egg fasteners, the P2 resonance frequency of the wheel–rail system decreased from 63 Hz to 31.5 Hz. Conversely, the use of floating slabs had a minimal effect on the P2 resonance frequency, with the peak remaining at 63 Hz; this is similar to turnouts that do not employ vibration mitigation measures. However, floating slabs may amplify low-frequency vibrations around 8 Hz.

When trains pass rapidly over frozen joints and fixed frogs, significant wheel–rail impacts may occur. However, welded joints and movable point rails can significantly reduce the associated environmental vibrations. The damping effect of the Cologne-egg fasteners can reach 7–14 dB, a fact that is attributed not only to the damping properties of the fasteners but also to the larger cross-sectional area of the tunnel walls.

It was also found that when a train decelerates while traversing a turnout, the vibration levels on the tunnel wall increase as the first three carriages pass, but then gradually decrease for subsequent carriages. The initial increase in vibration is caused by the superposition of vibrations from multiple carriages passing through the turnout, while the reduction in vibration levels for later carriages is due to the decreasing train speed.

This study provides data to support control measures for environmental vibrations in turnout areas of urban rapid rail transit lines. Future research should focus on optimizing turnout structures to reduce vibration and on implementing new vibration reduction measures.

Acknowledgments

This work is supported by the National Natural Science Foundation of China (Nos. U2568212, 52388102, 52478474, and 52472458), the Sichuan Science and Technology Program (Nos. 2025NSFTD0013, 2024NSFSC0003, and 2025YFHZ0035), and the National Key R&D Program of China (Nos. 2023YFB2604304, 2023YFB2604302, and 2023YFB2604303).

Author contributions

Zhaoguang ZHENG conceived and designed the research. Zihan ZHOU and Zeyu LIU were responsible for data processing. Jiayi HU contributed to text editing. Jingmang XU provided guidance on the structure and organization of the manuscript. Jiayin CHEN revised and polished the final version. Ping WANG provided project administration and overall coordination.

Conflict of interest

Zhaoguang ZHENG, Zihan ZHOU, Jingmang XU, Zeyu LIU, Jiayi HU, Jiayin CHEN, and Ping WANG declare that they have no conflict of interest.

References

Auersch L, Said S, Mueller R, 2017. Measurements on the vehicle-track interaction and the excitation of railway-induced ground vibration. Procedia Engineering, 10th International Conference on Structural Dynamics (EURODYN).

Bao XH, Xia ZF, Ye GL, et al., 2017. Numerical analysis on the seismic behavior of a large metro subway tunnel in liquefiable ground. *Tunnelling and Underground Space Technology*, 66:91-106. https://doi.org/10.1016/j.tust.2017.04.005

Bruni S, Anastasopoulos I, Alfi S, et al., 2009. Effects of train impacts on urban turnouts: modelling and validation through measurements. *Journal of Sound and Vibration*, 324(3-5):666-689.
https://doi.org/10.1016/j.jsv.2009.02.016

Chen J, Geng JL, Gao GY, et al., 2022. Mitigation of subway-induced low-frequency vibrations using a wave impeding block. *Transportation Geotechnics*, 37:100862.
https://doi.org/10.1016/j.trgeo.2022.100862

Connolly DP, Kouroussis G, Woodward PK, et al., 2014. Field testing and analysis of high speed rail vibrations. *Soil Dynamics and Earthquake Engineering*, 67:102-118.
https://doi.org/10.1016/j.soildyn.2014.08.013

Connolly DP, Marecki GP, Kouroussis G, et al., 2016. The growth of railway ground vibration problems−a review. *Science of the Total Environment*, 568:1276-1282.
https://doi.org/10.1016/j.scitotenv.2015.09.101

Daubechies I, Lu JF, Wu HT, 2011. Synchrosqueezed wavelet transforms: an empirical mode decomposition-like tool. *Applied and Computational Harmonic Analysis*, 30(2): 243-261.
https://doi.org/10.1016/j.acha.2010.08.002

Gao X, Yi Q, Lei JX, et al., 2023. Experimental study on the characteristics of vibration energy propagation in the subway turnout area. *Construction and Building Materials*, 409:134210.
https://doi.org/10.1016/j.conbuildmat.2023.134210

Gao X, Zhao CY, Yang Y, et al., 2024. Long-term efficient control of structure-borne noise inside buildings caused by underground railways by using novel damping fasteners. *Transportation Research Record*, 2678(2):635-653.
https://doi.org/10.1177/03611981231175896

Guo W, Bai ZY, Wang XB, et al., 2020. A combination strategy of hollow-closed-wall in-filled trench and elastic bearing for reducing environmental vibration induced by high-speed train. *Soil Dynamics and Earthquake Engineering*, 133:106136.
https://doi.org/10.1016/j.soildyn.2020.106136

Huang HY, Zhao MJ, Rong Y, et al., 2021. Analysis of the vibration of the ground surface by using the layered soil: viscoelastic Euler beam model due to the moving load. *Mathematical Problems in Engineering*, 2021:6619197.
https://doi.org/10.1155/2021/6619197

ISO (International Organization for Standardization), 2016. Mechanical Vibration—Measurement of Vibration Generated Internally in Railway Tunnels by the Passage of Trains, ISO 10815-2016. ISO, Geneva, Switzerland.

Jiang BL, Ma M, Li MH, et al., 2019. Experimental study of the vibration characteristics of the floating slab track in metro turnout zones. *Proceedings of the Institution of Mechanical Engineers, Part F: Journal of Rail and Rapid Transit*, 233(10):1081-1096.
https://doi.org/10.1177/0954409719826824

Kouroussis G, Zhu SY, Olivier B, et al., 2019. Urban railway ground vibrations induced by localized defects: using dynamic vibration absorbers as amitigation solution. *Journal of Zhejiang University-SCIENCE A*, 20(2):83-97.
https://doi.org/10.1631/jzus.A1800651

Lai J, Xu JM, Wang P, et al., 2021. Numerical investigation of dynamic derailment behavior of railway vehicle when passing through a turnout. *Engineering Failure Analysis*, 121:105132.
https://doi.org/10.1016/j.engfailanal.2020.105132

Lei JX, Gao X, Wang YX, et al., 2024. Vibration characteristics of subway turnout area during vehicle deceleration and assessment of the model accuracy. *Measurement*, 231: 114566.
https://doi.org/10.1016/j.measurement.2024.114566

Lei LJ, Miao LC, Li C, et al., 2021. Locally resonant periodic wave barriers for vibration isolation in subway engineering. *KSCE Journal of Civil Engineering*, 25(4):1239-1251.
https://doi.org/10.1007/s12205-021-1097-3

Mathur S, 2020. Impact of transit stations on house prices across entire price spectrum: a quantile regression approach. *Land Use Policy*, 99:104828.
https://doi.org/10.1016/j.landusepol.2020.104828

Norgate SH, Cooper-Ryan AM, Lavin S, et al., 2020. The impact of public transport on the health of work commuters: a systematic review. *Health Psychology Review*, 14(2):325-344.
https://doi.org/10.1080/17437199.2019.1618723

Qu XY, Ma M, Li MH, et al., 2019. Analysis of the vibration mitigation characteristics of the ballasted ladder track with elastic elements. *Sustainability*, 11(23):6780.
https://doi.org/10.3390/su11236780

Sadeghi J, Vasheghani M, 2021. Safety of buildings against train induced structure borne noise. *Building and Environment*, 197:107784.
https://doi.org/10.1016/j.buildenv.2021.107784

Sang T, Zhao CY, Wang YH, et al., 2020. Vibration transmission characteristic analysis of the metro turnout area by constant-Q nonstationary Gabor transform. *Measurement and Control*, 53(9-10):1739-1750.
https://doi.org/10.1177/0020294020952466

Sheng T, Shi WX, Shan JZ, et al., 2020. Base isolation of buildings for subway-induced environmental vibration: field experiments and a semi-analytical prediction model. *The Structural Design of Tall and Special Buildings*, 29(16): e1798.
https://doi.org/10.1002/tal.1798

Sheng X, Jones CJC, Petyt M, 1999. Ground vibration generated by a load moving along a railway track. *Journal of Sound and Vibration*, 228(1):129-156.
https://doi.org/10.1006/jsvi.1999.2406

Sun HL, Chen AH, Shi L, et al., 2018. Dynamic responses of a twin-tunnel subjected to moving loads in a saturated half-space. *Mathematical Problems in Engineering*, 2018: 6949507.
https://doi.org/10.1155/2018/6949507

Sun QQ, Dias D, Guo XF, et al., 2019. Numerical study on the effect of a subway station on the surface ground motion. *Computers and Geotechnics*, 111:243-254.
https://doi.org/10.1016/j.compgeo.2019.03.026

Sun XJ, Ma M, Jiang BL, et al., 2022. Ground vibration from freight railway: environmental impact and potential mitigation measure at propagation path. *Environmental Science and Pollution Research*, 29(29):44364-44377.

https://doi.org/10.1007/s11356-022-18955-z

Takamatsu M, Futatsuka M, Sakurai T, et al., 1982. A study of the extent and scope of local vibration hazards in Japan. *Industrial Health*, 20(3):177-190. https://doi.org/10.2486/indhealth.20.177

Thompson DJ, 2010. Railway Noise and Vibration: Mechanisms, Modelling and Means of Control. Elsevier, Amsterdam, the Netherlands. https://doi.org/10.1016/B978-0-08-045147-3.X0023-0

Wang LC, Ping W, Zhao CY, et al., 2020. An experimental study on the characteristics of vibration source in urban rail transit turnouts. *Proceedings of the Institution of Mechanical Engineers, Part F: Journal of Rail and Rapid Transit*, 234(9):945-957. https://doi.org/10.1177/0954409719877772

Wang S, Xin T, Wang PS, et al., 2022. Numerical study on high-frequency effect of rail corrugation on subway-induced environmental vibrations. *Environmental Science and Pollution Research*, 29(53):80657-80668. https://doi.org/10.1007/s11356-022-21264-0

Wang SG, Ge J, Wang M, et al., 2015. Experimental study on key technologies of high-speed turnout. *Journal of the China Railway Society*, 37(1):77-82 (in Chinese). https://doi.org/10.3969/j.issn.1001-8360.2015.01.012

Wen FY, Ren ZS, Sun SG, et al., 2014. ANSYS/DYNA-based study on wheel-rail dynamics of high-speed wheel-turnout system. *Journal of the China Railway Society*, 36(3):14-18 (in Chinese). https://doi.org/10.3969/j.issn.1001-8360.2014.03.003

Xin T, Wang S, Gao L, et al., 2020. Field measurement of rail corrugation influence on environmental noise and vibration: a case study in China. *Measurement*, 164:108084. https://doi.org/10.1016/j.measurement.2020.108084

Xu JM, Wang J, Wang P, et al., 2020. Study on the derailment behaviour of a railway wheelset with solid axles in a railway turnout. *Vehicle System Dynamics*, 58(1):123-143. https://doi.org/10.1080/00423114.2019.1566558

Xu R, Li XC, Yang W, et al., 2019. Field measurement and research on environmental vibration due to subway systems: a case study in eastern China. *Sustainability*, 11(23): 6835. https://doi.org/10.3390/su11236835

Yang JJ, Zhu SY, Zhai WM, et al., 2019. Prediction and mitigation of train-induced vibrations of large-scale building constructed on subway tunnel. *Science of the Total Environment*, 668:485-499. https://doi.org/10.1016/j.scitotenv.2019.02.397

Zheng JY, Zhao CY, Shi DJ, et al., 2024. A method for support stiffness failure identification in a steel spring floating slab track of urban railway: a case study in China. *Journal of Zhejiang University-SCIENCE A*, 25(3):206-222. https://doi.org/10.1631/jzus.A2300085

Zheng ZG, Hu JY, Qian Y, et al., 2025. The influence of elastic pads deterioration in the fastening system on the dynamic characteristics of the vehicle-turnout system. *Engineering Failure Analysis*, 167:108936. https://doi.org/10.1016/j.engfailanal.2024.108936

Zhou SX, Qin Z, Sun R, et al., 2017. Study on influence of inter-vehicle longitudinal damper on dynamic performance of high-speed EMU. *Journal of the China Railway Society*, 39(6):20-27 (in Chinese). https://doi.org/10.3969/j.issn.1001-8360.2017.06.003

Zou C, Wang YM, Wang P, et al., 2015. Measurement of ground and nearby building vibration and noise induced by trains in a metro depot. *Science of the Total Environment*, 536: 761-773. https://doi.org/10.1016/j.scitotenv.2015.07.123

Electronic supplementary materials

Sections S1 and S2, Figs. S1–S4